Analytical and experimental investigation of rake contact and friction behavior in metal cutting

Emre Ozlu [a], Erhan Budak [a,*], A. Molinari [b]

[a] Faculty of Engineering and Natural Sciences, Sabanci University, Orhanli, Tuzla, 34956 Istanbul, Turkey
[b] Laboratoire de Physique et Mécanique des Matériaux, UMR CNRS 7554, Université Paul Verlaine-Metz, Ile du Saulcy, 57045 Metz, France

Keywords:
Machining
Friction
Contact model

A B S T R A C T

In this study, the friction behavior in metal cutting operations is analyzed using a thermomechanical cutting process model that represents the contact on the rake face by sticking and sliding regions. The relationship between the sliding and the overall, i.e. apparent, friction coefficients are analyzed quantitatively, and verified experimentally. The sliding friction coefficient is identified for different workpiece–tool couples using cutting and non-cutting tests. In addition, the effect of the total, sticking and sliding contact lengths on the cutting mechanics is investigated. The effects of cutting conditions on the friction coefficients and contact lengths are analyzed. It is shown that the total contact length on the rake face is 3–5 times the feed rate. It is observed that the length of the sliding contact strongly depends on the cutting speed. For high cutting speeds the contact is mainly sliding whereas the sticking zone can be up to 30% of the total contact at low speeds. From the model predictions and measurements it can be concluded that the sticking contact length is less than 15% for most practical operations. Furthermore, it is also demonstrated that the true representation of the friction behavior in metal cutting operations should involve both sticking and sliding regions on the rake face for accurate predictions. Although the main findings of this study have been observed before, the main contribution of the current work is the quantitative analysis using an analytical model. Therefore, the results presented in this study can help to understand and model the friction in metal cutting.

1. Introduction

The friction due to the contact between the workpiece and the cutting tool is one of the key subjects in machining research. It is well known that cutting involves three deformation zones. The primary shear zone, i.e. the shear plane, is responsible for the chip formation whereas in the secondary shear zone on the rake face the workpiece and tool are in a complex state of contact. The third region, on the other hand, is responsible for ploughing and flank contact. Numerous models have been proposed involving, analytical with thin [1] and thick [2] shear zone approaches, semi-analytical [3,4], and numerical (mostly FEM based) [5,6] methods. Two important inputs for these models are the material model parameters and the friction coefficient between the tool and the workpiece material. These two inputs can be considered to be independent of the cutting mechanics as they are related to the mechanical and physical properties of the materials. Identification of both properties is very critical for accurate modeling of the machining processes. The focus of this paper is on the friction characteristics in metal cutting operations.

Being a common topic in mechanics, friction has been extensively studied in basic sciences. However, machining researchers have also paid special attention to friction due to its importance in cutting processes. The early studies on the subject concluded that there is a direct relationship between the shear angle and the friction. Using minimum energy principle for the continuous type chips, Merchant [1] concluded a relationship between the shear angle and the rake face friction. Oxley, [2] on the other hand, included the strain hardening effect in the slip-line model. As another approach, the semi-analytical method known as the mechanics of cutting [3,4] relates the apparent friction coefficient to the rake angle, feed rate and the cutting speed, and uses them in force predictions. However, this approach may take longer testing time since high number of tests must be carried out depending on the ranges. Similar mechanistic models do not provide much insight about the friction behavior of the workpiece and tool couples. In FEM modeling [5,6] the researchers mostly focused on the material behavior and chip formation and lacks the importance of the friction conditions on the rake face. Lee and Shaffer [7] obtained a similar relationship by applying slip-line field theory to the orthogonal cutting. The solutions presented in

* Corresponding author. Tel.: +90 216 483 9519; fax: +90 216 483 9550.
E-mail address: ebudak@sabanciuniv.edu (E. Budak).

these studies have assumptions which do not accurately represent the friction behavior of the process. Based on the experimental observations, however, it has been well accepted that the overall (apparent) friction coefficient on the rake face decreases with the increasing rake angle. On the other hand, the effects of other parameters such as cutting speed or feed rate were not known that well. Eventually, Zorev [8] approached the problem by observing the normal pressure and shear stress distributions on the rake face, and proposed distribution forms for them. Basically, Zorev [8] proposed that the material exiting the primary shear zone reaches the rake face with such a high normal pressure that there is a sticking contact zone close to the tool tip. Due to the drop in the normal pressure, the contact state changes to the sliding (Coulomb) friction away from the tool tip on the rake face. This behavior is also verified by numerous researches in later studies [9–12] mostly by split-tool experiments measuring the normal pressure and shear stress distributions on the rake face. In a later study, Fang [13] concludes that the tool–chip friction decreases with increasing absolute value of negative rake angle and with increasing cutting speed, by applying slip-line field analysis.

Friction between two contacting bodies has several dependencies such as the material pair, temperature, pressure, and speed depending on the application ranges [14–17]. For instance, in a recent study, Philippon et al. [18] conducted several experiments in an original test setup in order to investigate the sliding friction behavior at high sliding velocities, and concluded that the sliding coefficient of friction strongly depends on the speed and the pressure. In a different study Moufki et al. [14] proposed an orthogonal cutting model which relates the sliding friction coefficient to the mean temperature on the rake face.

A recent study [17] proposed an analytical orthogonal cutting model, which considers the sticking and sliding friction regions on the rake face and uses Johnson-Cook (JC) constitutive model. The JC constitutive relation is relatively simple, one dimensional model that accounts for the effects of strain, strain rate, and thermal softening on flow stress utilizing von Mises yield criterion. It describes the material hardening behavior based on the well-known power-law function. Also, this empirical relation is relatively simple to calibrate for a given material. It is relatively easy to implement into computer codes, inexpensive to use, and produces reasonably accurate predictions for a range of materials if the loading conditions do not exceed those used during the parameter identification tests. In the model [17], the sliding friction coefficient is related to the friction speed, and calibrated using a small number of orthogonal cutting tests, where the JC parameters are also calibrated for the given cutting speed range. The proposed model has both calibration and prediction capabilities.

Accurate representation of contact behavior on the rake face is critical for the thorough understanding and modeling of the metal cutting operations. In this regard, quantitative analysis of the friction behavior in metal cutting is important for better understanding of the nature of the process. The identification of the sliding friction coefficient between the workpiece–tool couple and the relation of the sliding friction coefficient to the apparent one is critical for process modeling. The contact lengths which are basically the physical representations of the friction behavior on the rake face, must also be modeled and analyzed. Based on these, the objective of this study is to further investigate the friction behavior in metal cutting operations. The focus of the study in this paper is on the mechanical behavior rather than micro-structural investigation. For this purpose, the rake contact model presented in [17,19] is used throughout this paper.

2. Thermomechanical dual-zone model

In this section, the cutting model which is used in this study is briefly presented. Although the dual-zone model detailed formulation applied to the orthogonal cutting conditions can be found in the Appendix, the detailed formulation for the oblique cutting conditions can be found in [19]. In this model, the contact between the chip and the tool on the rake face is represented by a dual-zone approach. Basically, the contact is divided into the sticking and a sliding friction region, which was originally proposed by Zorev [8] (see Fig. 1). In the first region, the contact condition is plastic due to the high normal pressure exerted on the tool, whereas in the second region the contact is elastic which can be represented by the sliding friction. There are two different friction coefficients that are defined on the rake contact. The apparent friction coefficient μ_a is due to the total cutting forces acting on the rake face. The sliding friction coefficient μ, on the other hand, is only due to the forces acting on the sliding region on the rake face.

The normal pressure distribution on the rake face is needed for the formulation of forces. The following distribution is selected as it is used and verified by several studies [10,11,14]

$$P(x) = P_0\left(1 - \frac{x}{\ell_c}\right)^{\zeta} \tag{1}$$

where ℓ_c is the total contact length, x the distance on the rake face from the tool tip, and ζ an exponential constant which represents the distribution of the pressure, and is selected as 3 in the current study based on the analysis of the split-tool test results [10,11]. It can be observed from Fig. 1, that the shear stress on the rake face is equal to the shear yield stress of the material (τ_1) along the sticking region with length ℓ_p. In addition, the shear stress in the sliding region is equal to the product of the sliding friction coefficient (μ) and the normal stress (P), according to the Coulomb friction law. Therefore, the mathematical representation of the shear stress distribution on the rake face can be defined as follows:

$$\tau = \begin{cases} \tau_1 & x \le \ell_p \\ \mu P & \ell_p \le x \le \ell_c \end{cases} \tag{2}$$

The three important outputs of the model is the total contact length ℓ_c, the sticking length ℓ_p, and the relationship between the sliding and sticking friction coefficients [19]

$$\ell_c = f\frac{\zeta - 2\sin(\phi_n - \lambda_a - \alpha_n)}{2 \quad \sin\phi_n \cos\lambda_a \cos\eta_c} \tag{3}$$

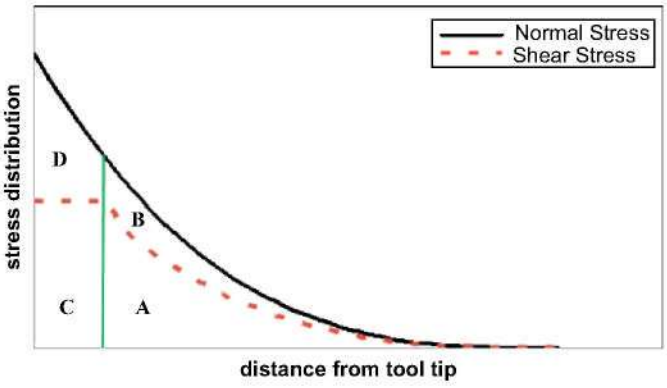

Fig. 1. Stress distributions on the rake face.

$$\ell_p = \ell_c \left(1 - \left(\frac{\tau_1}{P_0 \mu} \right)^{\frac{1}{\zeta}} \right) \tag{4}$$

$$\mu_a = \tan(\lambda_a) = \frac{\tau_1}{P_0} \left(1 - \varsigma \left(1 - \left(\frac{\tau_1}{P_0 \mu} \right)^{1/\varsigma} \right) \right) \tag{5}$$

where

$$\frac{\tau_1}{P_0} = \frac{\ell_c}{f(\zeta - 1)} \frac{\sin\phi_n \cos\eta_c \cos(\phi_n - \lambda_a - \alpha_n)}{\cos\eta_s \cos\lambda_a} \tag{6}$$

In the above equations, f is the uncut chip thickness, λ_a the friction angle, ϕ_n the normal shear angle, η_c the inclination angle, η_s the chip flow angle, and α_n the normal rake angle.

The proposed contact model can be used with any primary shear zone model provided that the shear stress at the exit of the shear zone is calculated accurately. For the analysis and predictions conducted in this study, the thermomechanical primary shear zone model proposed by [20,21] is used. The main assumption in modeling the primary shear zone is that the shear plane has a constant thickness, and that no plastic deformation occurs before and after the shear plane up to the sticking region on the rake face. In addition, it is assumed that the material behavior can be represented by the JC constitutive model. The material entering the primary shear zone sustains an initial shear stress value, and by the exit of the primary shear zone the shear stress evolves to τ_1 which is different from the initial value when inertia effects are important. Assuming a constant thickness of the shear zone and a uniform pressure distribution, the stress at the entrance of the shear band can be calculated iteratively. From the equations of motion for a steady state solution and a continuous type chip, the shear stress at the exit of the shear plane τ_1 can be calculated and used in the rake contact analysis as presented above. Other outputs of the model are the cutting forces, the shear stress, the normal pressure distribution on the rake face, and the shear angle.

3. Identification of sliding friction coefficient

In the foregoing analysis, there are two important inputs for the model: the material model parameters and the friction coefficient. Although the main focus of this study is on the friction behavior, choosing the correct material model parameters is another subject which is discussed in detail in [17,19]. However, it can be briefly stated that the dual-zone model can also be used to calibrate the material model coefficients. As for the friction, it should be noted that two friction coefficients are defined: the apparent and the sliding. If one of them is known the other can be calculated by using Eq. (5). As shown in [17] the dual-zone model can be used to calibrate these two inputs as well. The orthogonal tube cutting tests are used for calibration purposes as discussed in the following section. In addition, non-cutting friction tests were also conducted to compare with the sliding friction coefficients identified from the cutting tests, which is also discussed in the next section.

3.1. Identification of friction from orthogonal cutting tests

The proposed dual-zone model can be used to calculate the sliding friction coefficient between the tool and the workpiece material if the apparent friction coefficient is provided together with the cutting parameters and the material model coefficients. The calibration of the sliding friction coefficient between the tool and the workpiece material is done by orthogonal tube cutting tests. The tests are conducted on a lathe, where the orthogonal cutting conditions are satisfied by selecting inserts without inclination angles. Workpiece geometry is a tube in order to avoid the nose radius contact with the material. The test setup also involves a table type dynamometer and a DAQ system in order to collect the cutting force data. After each experiment the cut chip thickness is measured to identify the shear angle. The tests were conducted at different cutting speeds and feed rates. By the mechanics of cutting approach [3,4] the apparent friction coefficient on the rake face between the tool and the workpiece is calculated as follows:

$$\mu_a = \tan(\alpha_n + \tan^{-1}(F_f/F_t)) \tag{7}$$

where F_f and F_t are the measured feed and tangential (cutting) forces, respectively. The sliding friction coefficient μ is calculated by Eq. (5), and a function that relates μ to the chip velocity on the sliding region is obtained by data fitting techniques. The chip velocity along the sliding contact length is assumed to be uniform and is calculated as

$$V_{chip} = V \frac{\sin\phi}{\cos(\phi - \alpha)} \tag{8}$$

where V is the cutting speed.

Although the relationship between the apparent and the sliding friction coefficients is given by Eq. (5), we would like to discuss the relationship in a graphical manner here. In Fig. 1, the stress distributions are shown in order to discuss the sliding and apparent friction coefficients. Observing Fig. 1, the following mathematical representations for the friction coefficients can be deduced:

$$\mu = A/(A - B) \tag{9}$$

$$\mu_a = (A - C)/(A - B - C - D) \tag{10}$$

where A, B, C, and D are the areas under the curves. Since the area difference between the normal and shear stress under the sticking region is higher than the one in the sliding region, the value of μ_a must always be smaller than μ. This situation is always true for cases where the sliding friction is smaller than 1.

3.2. Identification of friction from non-cutting tests

In order to obtain the sliding coefficient of friction between the workpiece and the cutting tool materials independently from the cutting tests and the model, a non-cutting friction test setup is prepared (Fig. 2). This modified pin-on-disc setup is built on a manual lathe, and involves a dynamometer in order to measure the normal and the frictional forces, and a DAQ setup in order to collect the data. The contact between the tool and workpiece is realized by moving the tool with a fine slider in order to make the initial contact smoother. The sliding friction speed is controlled by the rotational speed of the work material and the radial position of the carbide rod with respect to the center of rotation. The sliding coefficient of friction is calculated using the mean values of

Fig. 2. The non-cutting friction test setup.

the friction ($F_{friction}$) and normal (F_{normal}) forces

$$\mu = F_{friction}/F_{normal} \tag{11}$$

Note again that the non-cutting friction tests are performed in order to compare the results with the identified friction coefficients from the cutting model, and they are not needed in regular identification procedure.

4. Results and discussions

In this section, the experimental results and the analysis of the friction behavior for different workpiece material and cutting tool couples are presented.

4.1. Friction test results

In this section, the sliding friction coefficients that are identified by the proposed model from the orthogonal tube cutting tests are presented, and discussed for two cases. In the first case, AISI 1050 steel with different cutting tools is presented, where in the second case AISI 4340 steel and Ti6Al4V alloy are investigated. All the cutting tests are conducted in orthogonal conditions with TPGN type tools, which are triangular with rake angle of 5° and without inclination and side edge cutting angles. Uncoated and coated carbide rods are used for non-cutting friction tests and the results are compared with the sliding friction coefficients obtained from the model using cutting tests data. Note that the non-cutting friction tests are not conducted for all the workpiece–tool couples. In all the tests conducted in this study the depth of cut is selected as 2 mm.

In the first case, the sliding friction coefficients between AISI 1050 steel and four different cutting tools were identified. The orthogonal cutting test parameters for those cases are presented in Table 1. Using the apparent friction coefficients identified from the tests, the sliding friction coefficients are determined by the model discussed in Section 3.1. The results can be found in Fig. 3.

Observing the results given in Fig. 3, it can be deduced that the friction characteristics are different for all the cutting tools. As can be seen in Fig. 3a, the sliding friction coefficient between the uncoated carbide tool and AISI 1050 steel does not depend on the friction speed strongly. But, there is a slight decrease in the sliding coefficient of friction at moderate speeds. However, for the ceramic (Fig. 3c) and CBN (Fig. 3d) tools, the sliding friction coefficient has almost a linear relationship with the friction speed where its value increases with the speed for the ceramic tool and decreases for the CBN tool. For the last cutting tool, the coated carbide, the sliding friction coefficient has a non-linear decreasing relationship with the friction speed. For this tool, the sliding friction coefficient drastically decreases from 0.7 (at slow cutting speeds) to 0.3 (at high cutting speeds).

Another interesting conclusion is that the sliding friction coefficients obtained from non-cutting friction tests have a very close agreement with the ones obtained from the cutting model and the tests. It should be noted that the average pressure on the rake face during cutting (200–600 MPa) is higher than the pressure applied during non-cutting tests (50–150 MPa). This observation suggests that the pressure may not affect the sliding friction strongly for these material–tool couples.

A final observation from the data presented in Fig. 3 is that the sliding friction decreases with the friction speed for all the tools except the ceramic insert. The reduction of the sliding friction coefficient with the speed can be attributed to the increased temperature at the contact. However, there is a need for further investigation in order to explain the different friction behavior of ceramic tools.

In the second case, two different workpiece material types are investigated: AISI 4340 steel with uncoated carbide tool and Ti6Al4V alloy with HSS cutting tool. The orthogonal cutting conditions can be found in Table 1, and the results can be seen in Fig. 4. The sliding friction coefficient between AISI 4340 steel and uncoated carbide tool (Fig. 4a) has a decreasing trend with the friction speed from 0.55 to 0.3. However, at higher speeds it takes almost a constant value of 0.35. On the other hand, the sliding friction coefficient between Ti6Al4V alloy and HSS cutting tool has a linear relationship with the speed and the average value is 0.35. Comparing the results of AISI 1050 (Fig. 3a) and AISI 4340 steel (Fig. 4a) with uncoated carbide tool, it can be concluded that AISI 4340 steel has a lower sliding friction coefficient. This can be attributed to the fact that the test materials had different hardness values. AISI 1050 steel had an average surface hardness of 190 BHN whereas it was 240 BHN for AISI 4340 steel.

4.2. Contact lengths and friction coefficients

The identification of sliding friction provides an important input for the analysis of the cutting process as discussed in the previous section. However, for the thorough analysis of the cutting process, one needs to analyze the apparent friction coefficient as well. The length of the sticking contact region on the rake face is one of the key parameters that determine the value of the apparent friction coefficient. Observing Eqs. (3) and (4), it can be deduced that the sticking contact length is a function of the feed rate (uncut chip thickness), shear stress at the exit of the primary shear band, the pressure distribution on the rake face, the rake and shear angles, and the apparent and sliding friction coefficients. As the relationship between the sticking length and the feed rate is linear, an increase in the feed rate directly affects the length of the contact. This was also verified experimentally [17]. The effect of the cutting velocity, on the other hand, is indirect, but can be predicted using the process model, and can also be observed experimentally. Eq. (4) shows that the sticking length depends on the sliding friction coefficient and the ratio τ_1/P_0 which are both affected by the cutting speed. In general, higher cutting speeds result in reduced sliding friction coefficients, and thus shorter sticking lengths. For instance, the sliding friction coefficient values of AISI 1050 steel with coated carbide tool (see Fig. 3b) decreases with the increasing friction speeds. Therefore,

Table 1
The material and cutting parameters used during the orthogonal cutting tests.

Cutting tool material	Workpiece material	Feed ranges (mm/rev)	Cutting speed ranges (m/min)
Uncoated carbide (P20)	AISI 1050	0.05–0.16	150–300
Coated carbide (TT1500)			150–600
Ceramic (AB30)			215–1225
CBN (TB650)			150–1225
Uncoated carbide (P20)	AISI 4340	0.05–0.3	80–500
HSS (T100)	Ti4Al6V	0.06–0.18	3–10

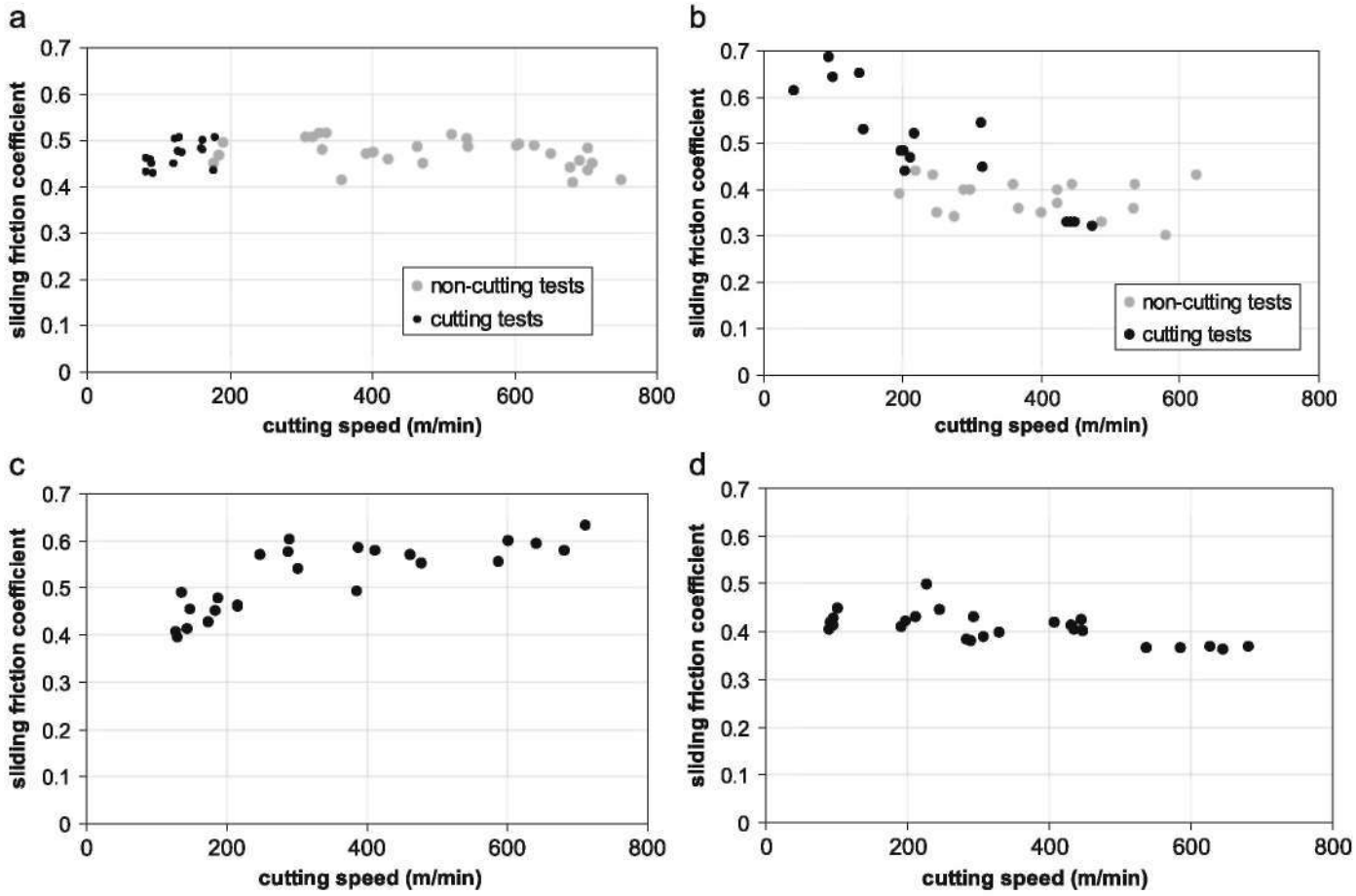

Fig. 3. Sliding friction coefficients between AISI 1050 steel and (a) uncoated carbide, (b) coated carbide, (c) ceramic, and (d) CBN tools with varying friction speeds.

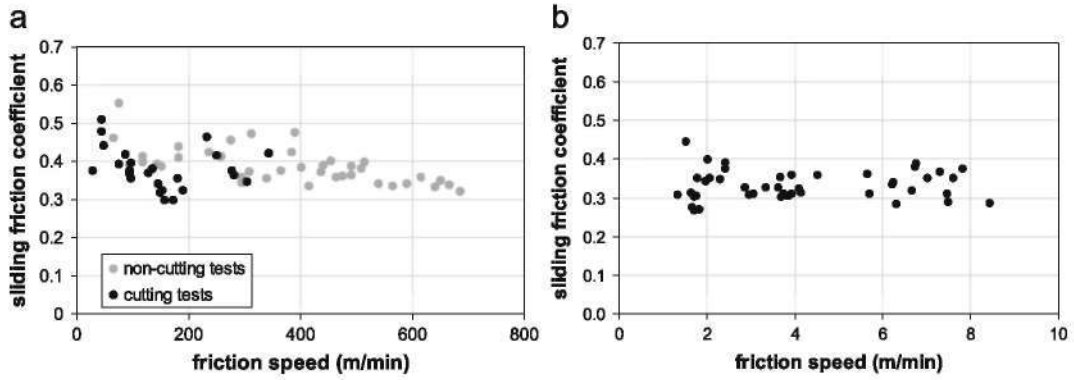

Fig. 4. Sliding friction coefficients between (a) AISI 4340 steel and uncoated carbide tool and (b) Ti6Al4V alloy with HSS cutting tool with varying friction speeds.

one should expect shorter sticking contact lengths at high cutting speeds.

Another observation on the friction behavior in metal cutting is the relationship between the sticking and sliding friction coefficients. As discussed in Section 3.1 the apparent friction coefficient is always smaller than the sliding friction coefficient. For instance for a constant total contact length and sliding friction coefficient (0.4 in this case), the variation of the ratio of the apparent and the sliding friction coefficient with the increasing sticking contact length can be obtained by Eqs. (5) and (6) as also shown in Fig. 5. As expected, when there is only sliding friction region present, i.e. at high cutting speeds ($\ell_p/\ell_c = 0$), the value of the sliding and apparent friction coefficients are equal to each other. On the other hand as the length of the sticking region increases, it results in lower apparent friction values than the sliding friction coefficient.

For further analysis of contact lengths, cutting experiments and simulations are conducted on the AISI 1050 steel with coated carbide and CBN cutting tools. The simulation results can be seen in Fig. 6. The length of the sticking region decreases by increasing cutting speed for each cutting tool as shown in Fig. 6. Especially for the coated carbide tool, the sticking zone vanishes, i.e. fully sliding contact, at the cutting speed of 600 m/min.

For the CBN tool on the other hand, fully sliding conditions are found to be present at cutting speeds higher than 1250 m/min as shown in Fig. 6b. In order to verify this behavior, the contact lengths for coated carbide tool were measured by using a microscope. Using optical methods is a simple and efficient way to characterize the contact length. After the cutting experiments are completed, the rake faces of the inserts are analyzed on a microscope. As can be seen in Fig. 7a the sliding marks can be defined very clearly. Therefore, the regions which do not have the sliding marks and are close to the tool tip are defined as the sticking region. The length of each region is determined by the geometrical measurement software available on the microscope. The images taken from the microscope measurements at cutting speeds of 100, 300, and 600 m/min can be seen in Fig. 7. As can be observed from the Fig. 7b and c, the length of the sticking zone at 100 m/min is longer than the sticking zone length at a cutting speed of 300 m/min. Fig. 7d indicates no evidence of sticking region at a cutting speed of 600 m/min. Therefore, the measurements verify the contact length predictions of the model.

4.3. Oblique cutting and rake contact behavior

The friction and rake face contact behavior in oblique cutting is always in the interest of the metal cutting researchers. For instance in mechanistic modeling of oblique cutting [4] it is recommended to use the shear stress, shear angle, and friction angle values obtained from the orthogonal cutting tests. Since the focus of this study is on the friction behavior, the friction behavior in oblique cutting is investigated in this section.

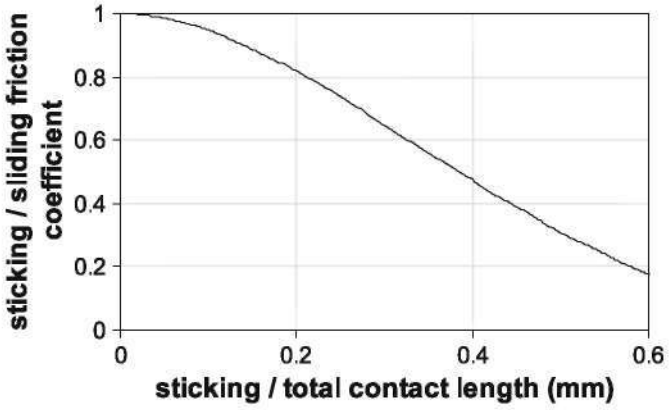

Fig. 5. The variation of the apparent friction coefficient with the sticking contact length for a constant total contact length.

Simulations are conducted for AISI 1050 steel and coated carbide tool couple. In the simulations 0° rake angle, 100 m/min cutting speed, 0.1 mm/rev feed rate are selected with varying inclination angle. The sliding friction coefficients calibrated from the orthogonal cutting tests are used during the simulations. As the sliding friction coefficient for AISI 1050 steel with coated carbide tool varies with the chip velocity, we would also like to see a similar effect on the friction behavior due to the inclination angle. However, as can be seen from Fig. 8a, the chip velocity varies only slightly with the inclination angle, and thus so should the sliding friction. This is verified by the calculations which show a constant sliding friction coefficient with the varying inclination angle as can be seen in Fig. 8b. It is also observed that the apparent friction angle does not vary with the inclination angle either, as shown in Fig. 8b. In order to investigate this behavior further, the total and the sticking contact lengths are analyzed and shown in Fig. 8c. As can be clearly seen from this figure, the total and the sticking contact lengths almost stay constant with the varying inclination angle. Since the percentage of the sticking length over the total contact length remains the same, it can be stated that the apparent friction coefficient does not change with the inclination angle.

The case simulated above is specific for AISI 1050 steel and coated carbide tool. It should be noted that the sliding friction behavior of this couple is drastically affected by the chip velocity. However, as it is also shown in Fig. 8a the chip velocity does not vary with the inclination angle significantly. Also, it is shown for the couple whose sliding friction coefficient varies strongly with the chip velocity that the apparent friction coefficient does not change with the inclination angle. Therefore, it can be concluded that the apparent friction coefficient is not affected by the inclination angle for the other material–tool couples whose sliding friction coefficients do not vary with the chip velocity that much or even remains constant.

4.4. Rake angle and friction

It is a well known phenomenon that the apparent friction coefficient increases with increasing rake angle. In this section this behavior is investigated quantitatively. Simulations using the proposed model at [17,19] are conducted for AISI 1050 steel with coated carbide tool for different rake angles at 300 m/min cutting speed and 0.1 mm/rev feed rate. The relationship obtained between the rake angle and the apparent friction coefficient can be seen in Fig. 9. As expected, the apparent friction coefficient increases with the increasing rake angle which can be explained by the variations of the friction and the normal forces on the rake face as shown in Fig. 10. The variations show that the normal cutting force decreases 41% whereas the

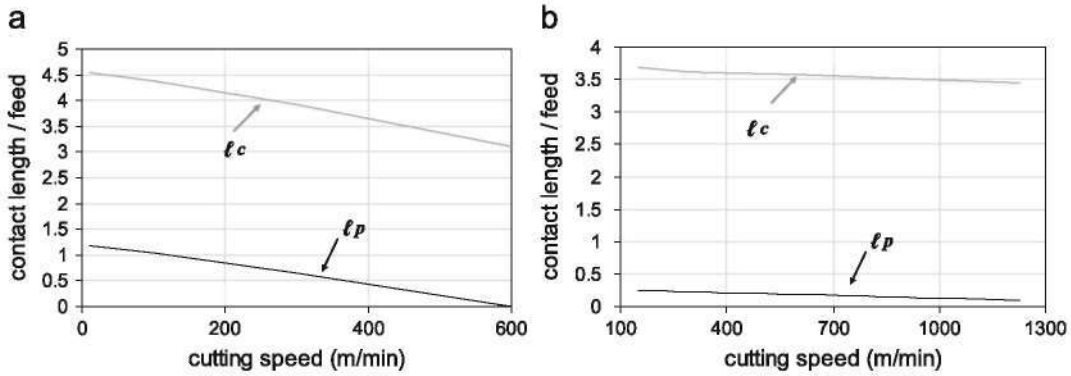

Fig. 6. The predicted variation of the ratio of the contact length and feed for AISI 1050 steel with (a) coated carbide and (b) CBN cutting tools.

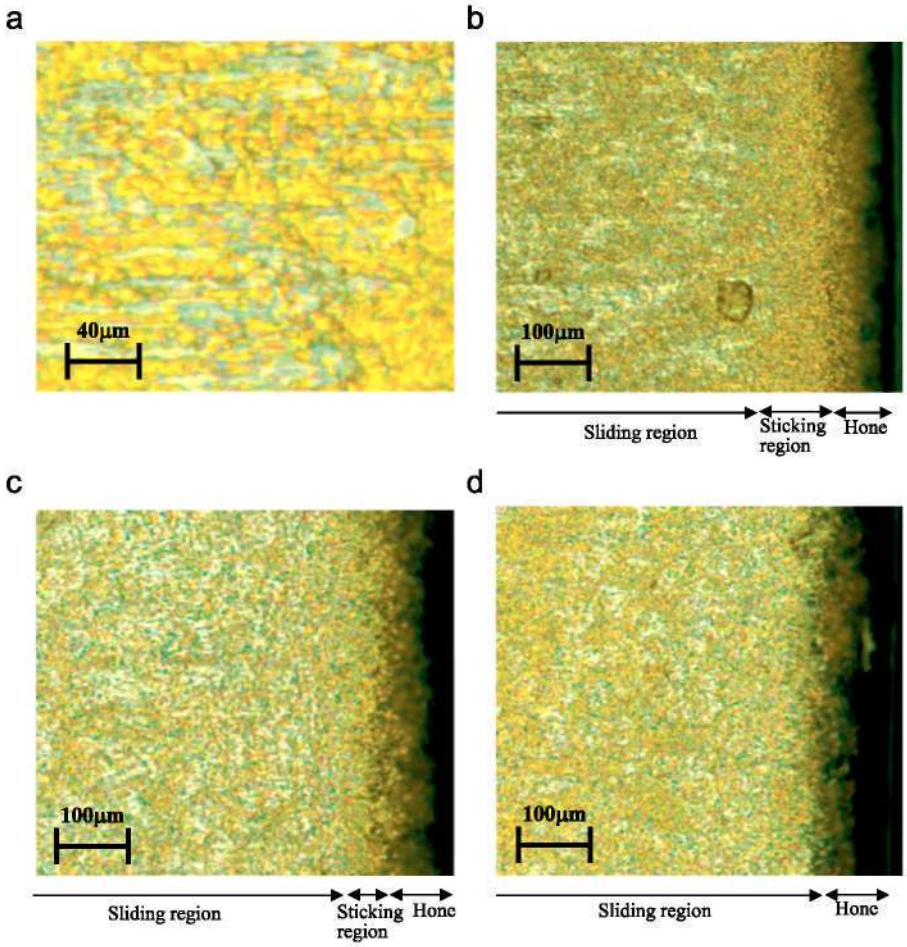

Fig. 7. (a) The sliding marks at 500 magnification, and rake face view of the tests at 200 magnification with a feed rate of 0.3 mm/rev and cutting speeds of (b) 100 m/min, (c) 300 m/min, and (d) 600 m/min.

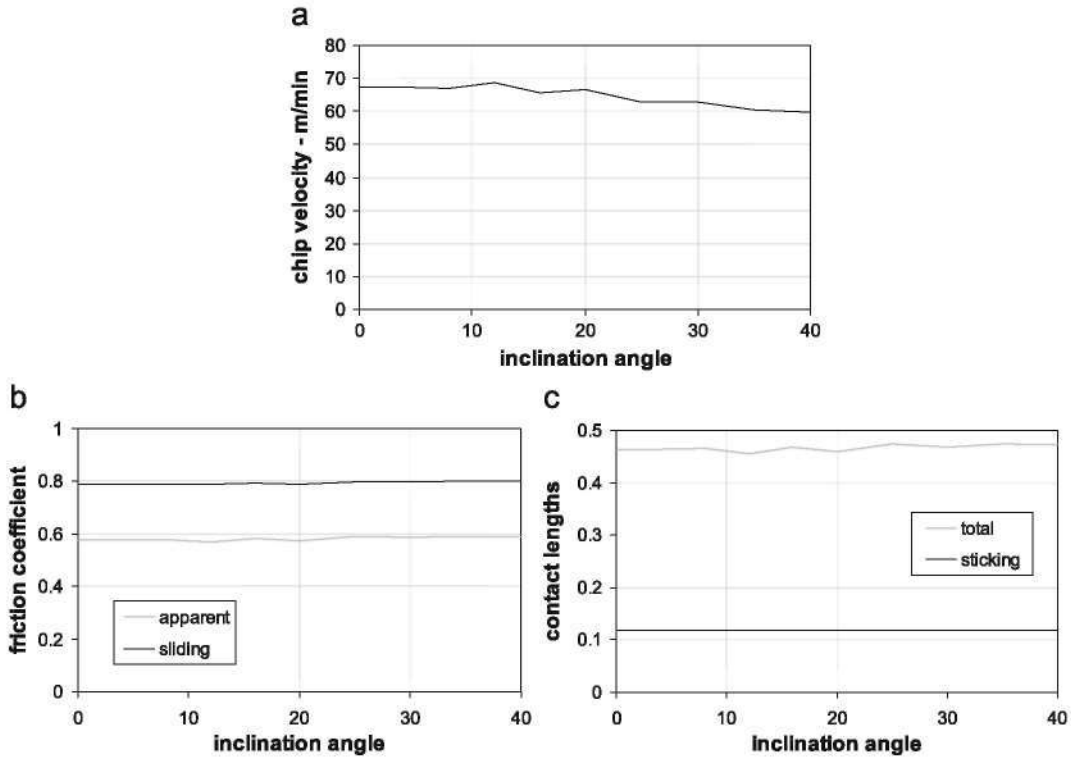

Fig. 8. (a) Chip velocity, (b) friction coefficients, and (c) contact lengths variations with the inclination angle.

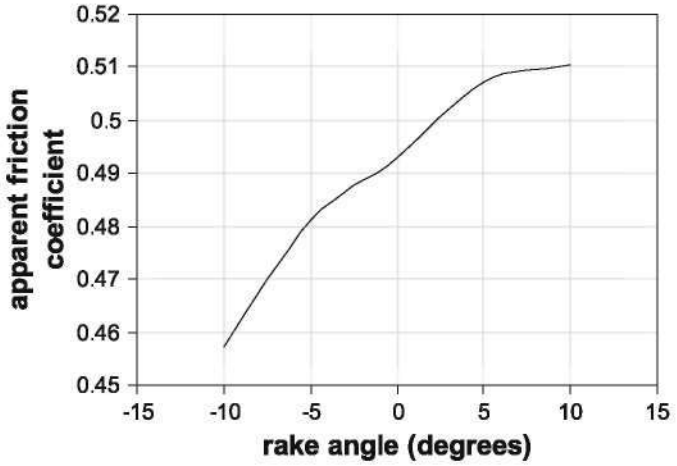

Fig. 9. The apparent friction coefficient variation with the rake angle for AISI 1050 steel using coated carbide tool.

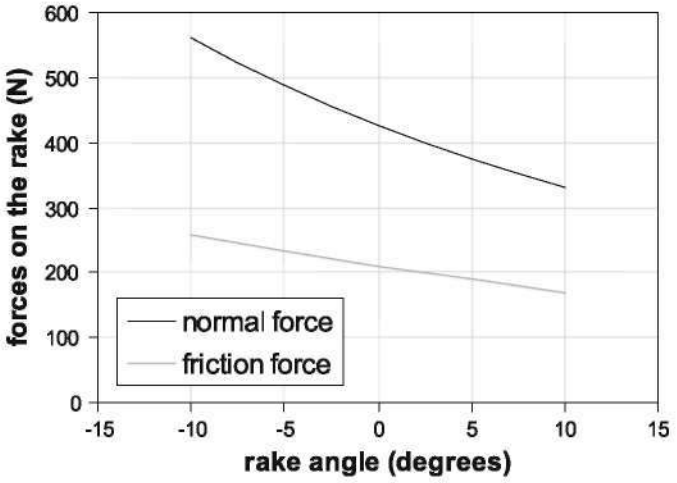

Fig. 10. The cutting forces variation with the rake angle for AISI 1050 steel using coated carbide tool.

friction force decreases 34% as the rake angle increases from −10° to 10°. Therefore, the apparent friction always increases with the rake angle.

The reason for the variation patterns for the forces on the rake can be attributed to several reasons. First of all the apparent friction coefficient is highly related to the contact lengths. Observing Eqs. (3) and (4), it can be stated that the relationship between the contact lengths and the rake angle is not explicit since the shear stress and the shear angle at the shear band, and the pressure distribution at the rake face are also affected by the rake angle. However, using the proposed model, the variation of the ratio of the sticking to total contact length with the rake angle can be determined (Fig. 11). It is seen that this ratio decreases with the increasing rake angle which means that the relative length of the sticking contact region with respect to the total contact length decreases with the increasing rake angle. This is due to the decrease in the normal force on the rake face as shown in Fig. 10. As discussed in Section 3.1, increasing sticking contact length decreases the apparent friction coefficient. Therefore, it can be concluded that the increase in apparent friction coefficient with the rake angle is due to the increasing percentage of the sliding length over the total contact length which is verified quantitatively.

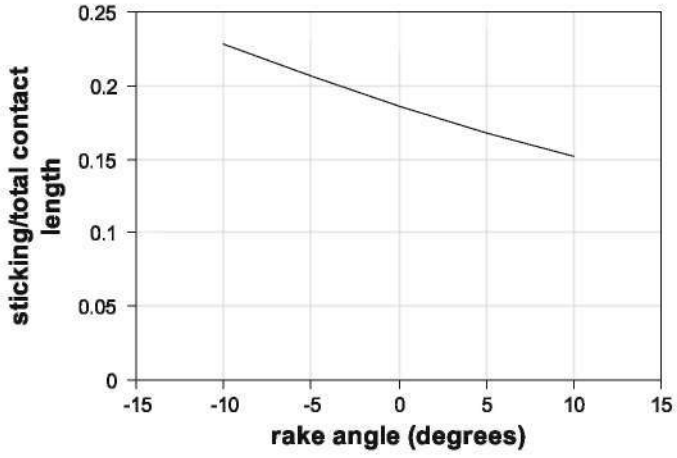

Fig. 11. The sticking-total contact length ratio variation with the rake angle for AISI 1050 steel using coated carbide tool.

Table 2
The friction models that are used in the comparative analysis for the prediction of the cutting forces.

Friction models	Shear stress distribution on the rake face	
I-Sticking+Sliding	$\tau = \tau_1$	$x < \ell_p$
	$\tau = \mu P$	$\ell_p \le x \le \ell_c$
II-Only sliding	$\tau = \mu P$	$0 < x < \ell_c$
III-Only sticking	$\tau = \tau_1$	$0 < x < \ell_c$

4.5. *Effect of friction model on cutting force predictions*

In this section, the effect of the friction modeling on the prediction of the cutting forces is discussed. Three different friction models that are listed in Table 2, are selected for comparative analysis. The first friction model involves the sticking and sliding contact regions on the rake face as defined by Eq. (2), which is used in all of the analysis throughout the study. The second model assumes that the friction on the rake face only consists of sliding friction. The last model, on the contrary, assumes that the friction state on the rake face is in sticking conditions. The models are used for cutting force predictions which are compared with the measurements.

In order to compare the cutting force predictions orthogonal cutting tests are conducted using AISI 1050 steel and coated carbide cutting tool. The proposed model of [17,19] which is briefly discussed in Section 2, is applied where the material model parameters and the sliding friction coefficient are calibrated. The cutting force predictions are done by using three different friction models listed in Table 2, and the results are given in Fig. 12 in terms of the error in the model predictions compared to the experiment results. The error is calculated as follows:

$$error = 100\frac{F_{\exp} - F_{sim}}{F_{\exp}} \tag{12}$$

where $F_{\exp}$ is the experimentally measured cutting force and F_{sim} is the cutting force calculated by the related model.

As can be observed from Fig. 12a, the prediction error in complete sliding friction assumption case decreases drastically with the increasing cutting speed. As also discussed in Section 4.2, at 600 m/min cutting speed the friction state is found to be fully sliding considering the length of the sticking region (see Figs. 6a and 7d). Supporting this observation, at a cutting speed of 606 m/min, the predictions are very close to the experimental

measurements. Therefore, it is an expected result that the model which assumes only sliding friction on the rake face yields better predictions at high cutting speeds. On the contrary, when complete sticking on the rake face is assumed the prediction error becomes higher as the cutting speed increases. The error at slow cutting speeds is lower (Fig. 12a) indicating longer sticking zone at those speeds as shown in Figs. 6 and 7 as well. However, even at slow speeds the prediction error is quite high which suggests that the rake contact cannot be modeled accurately using sticking only. This can also be seen clearly in Fig. 6 that the sliding zone always exists even at slow cutting speeds. On the other hand, the friction model which considers both sticking and sliding regions provides very close predictions to the experimental measurements since it represents the true friction behavior in cutting operations.

As can be seen from Fig. 12, the prediction error for the cutting (tangential) force is drastically lower than that for the feed force when fully sliding or fully sticking conditions are assumed in friction modeling. Similar results are also observed in the FE cutting process simulations [22]. This is due to the fact that the cutting force mainly depends on the material behavior in the primary shear zone whereas the feed force depends more on the friction behavior on the rake face. Thus, unrealistic modeling of the friction behavior affects the accuracy of feed force predictions strongly.

5. Conclusions

In this study, an investigation of the rake contact and friction behaviors in metal cutting operations is performed. Although the main findings of this study have been observed by several researchers before, the main contribution is that these observations are explained by quantitative analysis, and now they can be represented by an analytical model. The analyses are carried out with a thermomechanical analytical model that considers a dual-zone contact behavior on the rake face. Specifically, it is demonstrated that the accurate cutting force predictions can only be obtained by considering the true nature of the contact on the rake face, i.e. by including both sticking and sliding zones in the analysis. The thermomechanical process model was also used to identify the effects of the cutting conditions on the rake contact and the friction, based on the experimental data. The following are the main observations obtained from the analytical and experimental analyses.

- The total contact length increases by the feed rate and decreases by the cutting speed. For AISI 1050 steel and coated carbide tool, the total contact length decreases with the speed up to 30% whereas this ratio is about 10% for CBN tools.
- The apparent friction coefficient strongly depends on the relative lengths of the sticking and sliding zones, and the sliding friction coefficient. It is shown that the apparent friction coefficient is always smaller than the sliding friction coefficient. Although this depends on the cutting speed, the difference between both the coefficients is around 20% in most applications.
- The sticking contact length is strongly affected by the cutting speed. For some material–tool couples, it is observed that the contact is almost completely sliding at high cutting speeds which are 600 m/min for the coated carbide, and over 1200 m/min for the CBN tool. For slow and moderate cutting speeds the contact involves both sticking and sliding zones. However, even at slow speeds the contact is mainly in the elastic, i.e. sliding, state. For most practical cutting conditions the sticking contact length is less than 15% of the total contact.
- Based on the cases considered in this study, it can be concluded that the total and sticking contact lengths are approximately 3–5 and 0–1.5 times the feed rate, respectively, both decreasing with the cutting speed.
- It is quantitatively shown that the reason for the apparent friction coefficient to increase with the rake angle is due to the decrease of the sticking contact length percentage in the total contact length. For the coated carbide tool having -10° rake angle this ratio is 22%, where it is 15% for the case where the rake angle is 10°.
- It is demonstrated that the sliding and apparent friction coefficients are not affected by the inclination angle. The reason is again explained quantitatively by showing that the contact lengths are not affected by the inclination angle. Therefore, it is concluded that the friction coefficients obtained from orthogonal tests can be used for the analysis of oblique cutting.
- The sliding friction coefficients for various material–tool couples are identified and can be used for further studies. The main parameter that affects the sliding friction coefficient is observed to be the friction speed. For AISI 1050 steel and uncoated carbide tool couple the sliding friction coefficient is found to be varying between 0.4 and 0.5 which is slightly affected by the cutting speed. For the coated carbide tool, on the other hand, a drastic change with the cutting speed is observed where the sliding friction value decreases from 0.7 (at 50 m/min) to 0.3 (at 600 m/min). In addition, the ceramic cutting tool shows a slight increase with the cutting speed where the CBN cutting tool shows a slight decrease.

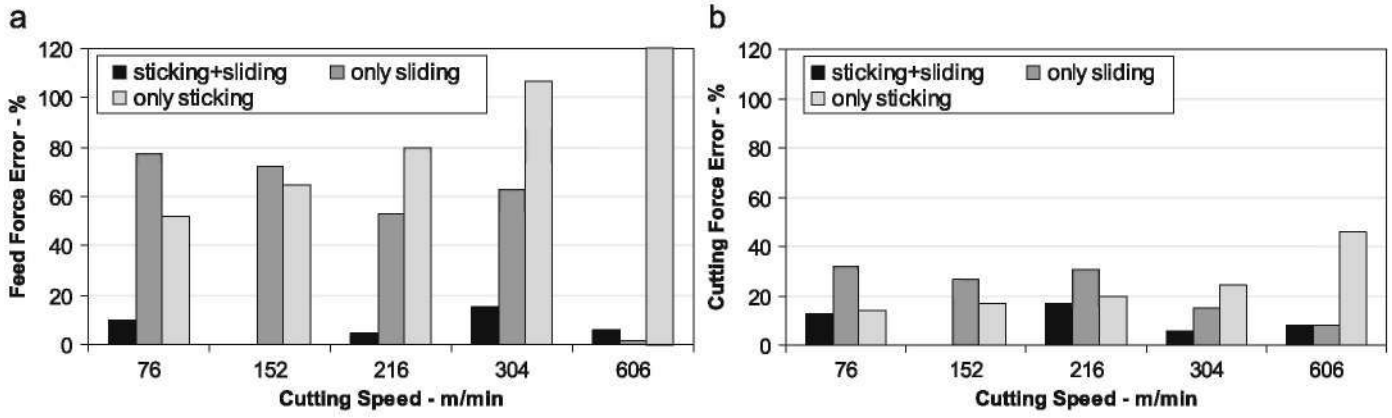

Fig. 12. The (a) feed force and (b) cutting force errors between the predictions using the different friction models and experimental results for AISI 1050 steel and coated carbide tool.

Appendix. The formulation of dual-zone model for orthogonal cutting conditions

In the appendix, the derivation of the dual-zone contact model for orthogonal cutting is given in detail. The distribution of the shear and normal stress on the rake face can be as indicated in Fig. A.1.

The shear stress distribution on the rake face can be defined as follows:

$$\begin{aligned} \tau &= \tau_1 \quad x \le \ell_p \\ \tau &= \mu P \quad \ell_p \le x \le \ell_c \end{aligned} \tag{A.1}$$

where ℓ_c is the contact length, and x is the distance on the rake face from the tool tip.

Also, for the normal stress on the rake face the following distribution is selected

$$P(x) = P_0\left(1 - \frac{x}{\ell_c}\right)^{\zeta} \tag{A.2}$$

where P_0 is the normal stress on the rake face at the tool tip, and ζ is the distribution exponent. From the coulomb friction law along the sliding zone we have:

$$\tau(x) = \mu P_0\left(1 - \frac{x}{\ell_c}\right)^{\zeta} \tag{A.3}$$

At the end of the sticking zone (beginning of the sliding zone) the tangential stress τ is equal to the shear yield stressτ_1

$$\tau_1 = \mu P_0\left(1 - \frac{\ell_p}{\ell_c}\right)^{\zeta} \tag{A.4}$$

From Eq. (A.4), the length of the sticking zone can be obtained as follows:

$$\ell_p = \ell_c\left(-\left(\frac{\tau_1}{P_0\mu}\right)^{1/\zeta} + 1\right) \tag{A.5}$$

For a given μ, there are three unknowns P_0, ℓ_p, and ℓ_c in Eq. (A.5). P_0 can be related to the normal force acting on the rake face by considering the pressure distribution along the contact length ℓ_c

$$N = \int_0^{\ell_c} P(x)\,dx = \int_0^{\ell_c} P_0\left(1 - \frac{x}{\ell_c}\right)^{\zeta} w\,dx = P_0\frac{w\ell_c}{\zeta + 1} \tag{A.6}$$

where w is the width of cut. The normal force N can also be calculated in terms of the shear force on the shear plane

$$N = F_s\frac{\cos\lambda_a}{\cos(\phi + \lambda_a - \alpha)} \tag{A.7}$$

where λ_a is the friction angle defined by $\lambda_a = \tan^{-1}\mu_a$. The apparent (global) friction coefficient μ_a is defined later, see (A.14). Also the shear force F_s in Eq. (A.7) is obtained by assuming that the shear stress distribution on the shear plane AB at the exit of the primary shear zone is uniform

$$F_s = \tau_1\frac{wh_1}{\sin\phi} \tag{A.8}$$

In this relationship, h_1 is the uncut chip thickness. Combining Eqs. (A.6–A.8) P_0 can be calculated as follows:

$$P_0 = \tau_1\frac{h_1(\zeta + 1)}{\ell_c\sin\phi}\frac{\cos\lambda_a}{\cos(\phi + \lambda_a - \alpha)} \tag{A.9}$$

The next step is to calculate the contact length ℓ_c. Assuming that the normal stress is distributed uniformly along the shear plane AB, and considering the momentum equilibrium at the tool tip, we get $M_{AB} = M_{BC}$ and

$$M_{AB} = F_n\frac{AB}{2} = F_sh_1\frac{\tan(\phi + \lambda_a - \alpha)}{2\sin\phi} \tag{A.10}$$

$$M_{BC} = \int_0^{\ell_c} xP_0\left(1 - \frac{x}{\ell_c}\right)^{\zeta} w\,dx = F_s\frac{\ell_c}{\zeta + 2}\frac{\cos\lambda_a}{\cos(\phi + \lambda_a - \alpha)} \tag{A.11}$$

From Eqs. (A.10) and (A.11), the contact length ℓ_c is obtained as follows:

$$\ell_c = h_1\frac{\zeta + 2}{2}\frac{\sin(\phi + \lambda_a - \alpha)}{\sin\phi\cos\lambda_a} \tag{A.12}$$

Considering the additional Eqs. (A.9) and (A.12), ℓ_p can be calculated by Eq. (A.5), for a given value of the shear angle ϕ.

It can be shown that along the sliding zone the Eq. (A.3) takes the form

$$\tau(x) = \tau_1\left(1 - \frac{x - \ell_p}{\ell_e}\right)^{\zeta} \quad \ell_p \le x \le \ell_c \tag{A.13}$$

where ℓ_e is the length of the sliding region, Fig. A.2b.

The only parameter left to be defined is the apparent friction coefficient, μ_a. The apparent friction coefficient is defined as follows:

$$\mu_a = F/N \tag{A.14}$$

The normal force N acting on the rake face can be obtained from Eq. (A.6) and the friction force F on the rake face can be

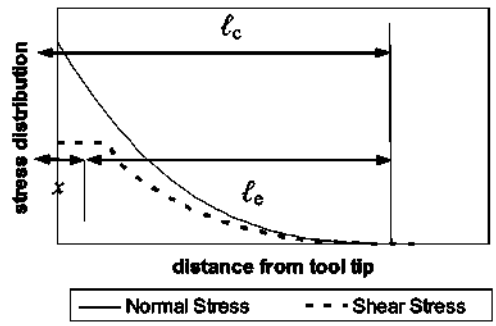

Fig. A.1. Stress distributions and contact lengths on the rake face.

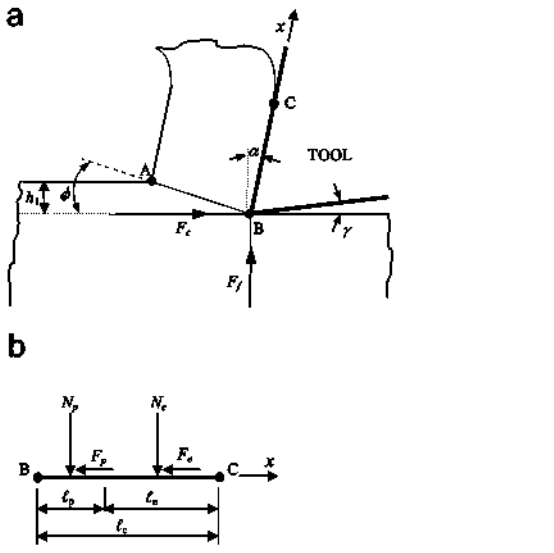

Fig. A.2. Schematic representation of (a) orthogonal cutting and (b) the forces acting on the rake face.

calculated as

$$F = \int_0^{\ell_p} \tau_1 w\, dx + \int_{\ell_p}^{\ell_c} \tau_1 \left(1 - \frac{x - \ell_p}{\ell_e}\right)^{\zeta} w\, dx = \tau_1 w \left(\ell_p + \frac{\ell_e}{\zeta + 1}\right) \tag{A.15}$$

Substituting Eqs. (A.6) and (A.15) into Eq. (A.14), μ_a has the form

$$\mu_a = \frac{\tau_1}{P_0} \frac{\ell_p(\zeta + 1) + \ell_e}{\ell_c} \tag{A.16}$$

When sticking occurs, the relationship (A.16) between the apparent (or global) and the local friction coefficients, respectively μ_a and μ can be written, by using (A.5) as follows:

$$\mu_a = \tan(\lambda_a) = \frac{\tau_1}{P_0} \left(1 + \varsigma \left(1 - \left(\frac{\tau_1}{P_0 \mu}\right)^{1/\varsigma}\right)\right) \tag{A.17}$$

where

$$\frac{\tau_1}{P_0} = \frac{\varsigma + 2}{4(\varsigma + 1)} \frac{\sin(2(\phi + \lambda_a - \alpha))}{(\cos \lambda_a)^2} \tag{A.18}$$

The latter relationship is obtained from Eqs. (A.9) and (A.12).

Moreover, the average normal pressure P_{avg} acting on the sliding region of the rake contact and can be calculated as follows:

$$P_{avg} = \frac{1}{(\ell_c - \ell_p)} \int_{\ell_p}^{\ell_c} P = \frac{P_o}{(\zeta + 1)} \left(\frac{\ell_c - \ell_p}{\ell_c}\right)^{\zeta} \tag{A.19}$$

Substitution of (A.18) into (A.17) provides the link between the apparent friction angle λ_a and the local friction coefficient μ, for a given value of ϕ.

References

[1] E. Merchant, Mechanics of the Metal Cutting Process I. Orthogonal Cutting and a Type 2 Chip, J. Appl. Phys. 16/5 (1945) 267–275.
[2] P.L.B. Oxley, Mechanics of Machining, an Analytical Approach to Assessing Machinability, Ellis Horwood Limited, England, 1989.
[3] E. Budak, Y. Altintas, E.J.A. Armarego, Prediction of milling force coefficients from orthogonal cutting data, Trans. ASME J. Man. Sci. Eng. 118 (1996) 216–224.
[4] Y. Altintas, Manufacturing Automation, Cambridge University Press, Cambridge, 2000.
[5] Y. Yen, A. Jain, T. Altan, A finite element analysis of orthogonal machining using different tool edge geometries, J. M. Pr. Tec. 146 (2004) 72–81.
[6] E. Ceretti, E. Taupin, T. Altan, Simulation of metal flow and fracture applications in orthogonal cutting, blanking, and cold extrusion, Ann. CIRP 46/1 (1997) 187–190.
[7] E.H. Lee, B.W. Shaffer, Theory of plasticity applied to the problem of machining, Trans. ASME J. Appl. Mech. 18 (1951) 405–413.
[8] N.N. Zorev, Inter-relationship between shear processes occurring along tool face and shear plane in metal cutting, in: International Research in Production Engineering, ASME, New York, 1963, pp. 42–49.
[9] J.A. Bailey, Friction in metal machining: mechanical aspects, Wear 31 (1975) 243–275.
[10] S. Kato, K. Yamaguchi, M. Yamada, Stress distribution at the interface between tool and chip in machining, J. Eng. Ind. 94 (1972) 683–689.
[11] G. Barrow, T. Graham, T. Kurimoto, F. Leong, Determination of rake face stress distribution in orthogonal machining, Int. J. Mach. Tools Des. Res. 22/1 (1982) 75–85.
[12] T.H.C. Childs, Friction modeling in metal cutting, Wear 260 (2006) 310–318.
[13] N. Fang, Tool–chip friction in machining with a large negative rake angle tool, Wear 258 (2005) 890–897.
[14] A. Moufki, A. Molinari, D. Dudzinski, Modelling of orthogonal cutting with a temperature dependent friction law, J. Mech. Phys. Solids 46/10 (1998) 2103–2138.
[15] Z. Tao, M.R. Lovell, J.C. Yang, Evaluation of interfacial friction in material removal processes: the role of workpiece properties and contact geometry, Wear 256 (2004) 664–670.
[16] W. Xie, E.C. De Meter, M.W. Trethewey, An experimental evaluation of coefficients of static friction of common workpiece-fixture element pairs, Int. J. Mach. Tools Manuf. 40 (2000) 467–488.
[17] E. Ozlu, E. Budak, A. Molinari, Thermomechanical modeling of orthogonal cutting including the effect of stick-slide regions on the rake face, 10th CIRP International Workshop on Modeling of Machining Operations, Calabria, Italy, August 2007.
[18] S. Philippon, G. Sutter, A. Molinari, An experimental study of friction at high sliding velocities, Wear 257 (2004) 777–784.
[19] E. Budak, E. Ozlu, Development of a thermomechanical cutting process model for machining process simulations, CIRP Ann. Manuf. Technol. 57 (2008) 97–100.
[20] A. Molinari, D. Dudzinski, Stationary shear bands in high speed machining, C. R. Acad. Sci. 315 (Série II) (1992) 399–405.
[21] D. Dudzinski, A. Molinari, A modeling of cutting for viscoplastic materials, Int. J. Mech. Sci. 39/4 (1997) 369–389.
[22] L. Filice, F. Micari, S. Rizzuti, D. Umbrello, A critical analysis on the friction modeling in orthogonal machining, Int. J. Mach. Tools Manuf. 47 (2007) 709–714.